それぞれ特徴的な転写因子やサイトカイン，ケモカイン受容体を発現している．通常，これらのThサブセットはバランスを保って存在しているが，そのバランスに破綻が生じると宿主に免疫異常がひき起こされると考えられており，近年，このバランス破綻にTh細胞の分化異常の重要性が注目されている[9]．これに関連して，われわれはHAMにおけるHTLV-1感染細胞が主にTregやTh2細胞に発現するケモカイン受容体CCR4陽性のCD4$^+$T細胞であり，興味深いことにHAMの末梢血CCR4$^+$CD4$^+$T細胞は，炎症性サイトカインIFN-γを産生するTh1細胞様の異常細胞に変化し増加していることを示した[10]．また，HTLV-1由来の機能遺伝子であるtaxやHBZの発現がTregの免疫制御機能の低下を誘導することが報告されている[11][12]．このようにHAM患者におけるCCR4$^+$CD4$^+$T細胞は，HTLV-1感染によって機能的な異常を伴って増加しており，Thバランスにも影響を与え，HAM病態形成に重要な役割を果たしていることが示唆されている．

HAMにおける炎症の慢性化機構

HAM脊髄病巣の病理所見では，小血管周囲の炎症細胞の浸潤やIFN-γなどの炎症性サイトカインの発現を認め，持続的な炎症が起こっていることが示されてきた[13]．さらに，HTLV-1感染細胞についてin situ PCR法を用いて解析されており，HTLV-1の感染は浸潤したT細胞にのみ確認され，周辺の神経細胞やグリア細胞には確認されていない[14]．以上から，HAMの脊髄病巣ではHTLV-1感染T細胞に起因する慢性炎症が存在すると考えられているが，その炎症の形成および慢性化機構については不明であった．

最近，われわれはHAM患者脊髄における炎症の慢性化が脊髄局所での病的なケモカイン産生を軸とする炎症のポジティブフィードバックループに起因するという仮説を立て，HAMの病態の主軸となるケモカインの同定を試みた[15]．その結果，HAM患者髄液中で高値を示した炎症性ケモカインの中で，Th1細胞に発現するCXCR3のリガンドであるCXCL10のみが，血清中よりも髄液中で高い濃度勾配を示し，髄液CXCL10濃度は髄液細胞数と相関していた．また，HAM患者の髄液や脊髄病変には，CXCR3を発現する細胞(主にCD4$^+$T細胞とCD8$^+$T細胞)が多数を占めており，CXCL10によりCXCR3陽性細胞が優先的に脊髄に遊走していることが示された．さらに，CXCL10により遊走するCXCR3$^+$CD4$^+$T細胞は，その一部にHTLV-1感染を認め，HTLV-1感染細胞の脊髄への遊走にもCXCL10が重要な役割を果たしていることが示唆された．また，患者脊髄病変部におけるCXCL10の主な産生細胞はアストロサイトであることが判明し，アストロサイトは患者由来CD4$^+$T細胞からのIFN-γ産生によりCXCL10を過剰産生することが示された．以上より，HAMの脊髄病変では浸潤したHTLV-1感染細胞から産生されるIFN-γによってアストロサイトからのCXCL10産生を刺激し，そのCXCL10はCXCR3陽性の感染CD4$^+$T細胞やCD8$^+$T細胞などの炎症細胞の脊髄への遊走を促し，それらの細胞がIFN-γを産生してアストロサイトからのさらなるCXCL10産生を刺激するという，炎症のポジティブフィードバックループ(IFN-γ-CXCL10-CXCR3ループ)の形成が炎症の慢性化機構の主軸であり，HAMの脊髄病巣の形成・維持に重要な役割を果たしていると考えられる(図2)[15]．

HAMに対する抗CCR4抗体療法の開発

上述したようなこれまでのHAMの病態研究や臨床的なデータから，HAM患者においてHTLV-1感染細胞の劇的な低下とその維持を実現することは，病態ならびに長期予後の改善につながることが予想され，HAMにおいて感染細胞を標的とした薬剤開発の必要性が高い．そのためこれまでも世界中の研究者がHAMに対する抗ウイルス療法の開発を試みてきた．逆転写酵素阻害薬やプロテアーゼ阻害薬などは*in vitro*での感染阻害作用が示され，実際にHAM患者を対象として臨床試験が実施されたが，ウイルス量の減少効果はまったく得られず，治療効果に乏しかった[16][17]．HTLV-1は，エイズウイルスや肝炎ウイルスなどとは異なり転写レベルが低いため血清中にウイルスが存在せず，また感染細胞はオリゴクローナルな集団を形成する特徴を有しているので[18][19]，ウイルス量の制御には異なった戦略，たとえば感染細胞を特異的に攻撃・死滅させる

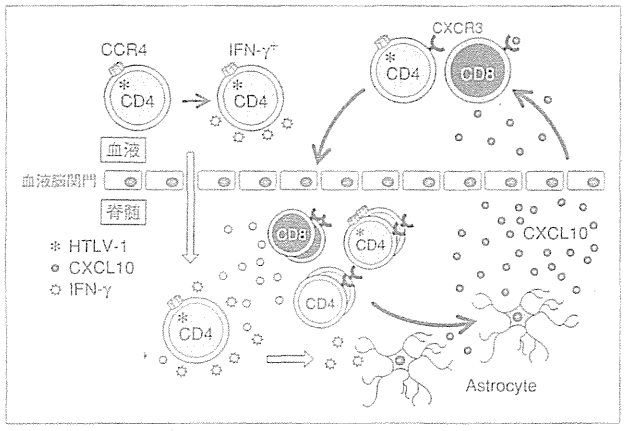

図2　HAM感染細胞を起因とした炎症のポジティブフィードバックループ

抗体療法などの開発が必要と考えられる．

そこでわれわれは，HAM患者においてHTLV-1が主にCCR4陽性T細胞に感染し，その細胞機能が炎症促進的になっていると報告したことなどを踏まえ[19]，CCR4抗原を標的として抗体依存性細胞障害活性を示すヒト化抗CCR4抗体製剤mogamulizumab(KW-0761)に着目して研究を進めた．KW-0761はわが国で開発され，HTLV-1感染者より発症する成人T細胞白血病・リンパ腫(ATLL)の治療薬として最近承認された薬剤である．われわれはKW-0761を用いて，HAM患者の血液・髄液由来細胞における感染細胞殺傷効果，自発的細胞増殖抑制効果，炎症性サイトカイン産生抑制効果等を証明し，CCR4がHAMの有用な治療標的分子であることを示した[20]．さらに，これまでのKW-0761を用いた他の治験において，健康成人やATL等患者に対する安全性が確認されており，またATL患者におけるCCR4陽性ATL細胞の劇的な減少効果が示されていることから[21][22]，KW-0761は，HAMに対する安全かつ有効な治療薬になりうると考えられた．そこで，KW-0761のHAMに対する医師主導治験の実施を計画した．試験デザインは，HAMが希少難病であることを踏まえ，できるだけ早期に新薬承認がなされるよう，第I/IIa相試験と工夫した．治験プロトコールの内容は，対象を既存治療で効果不十分なHAM患者とし，主要評価項目は安全性で，用量制限毒性の発現状況に基づき，最大耐用量を明らかにし，同時に薬物動態について検討する．また副次的に，抗感染細胞効果や歩行時間の非増悪期間などを検討して有効性を探索する．すでに治験プロトコールに関して医薬品医療機器総合機構(PMDA)の対面助言を終了しており，厚生労働省科学研究費補助金の助成のもと，2013年12月から治験を開始した．今回実施するKW-0761の治験が成功すれば，これまで有効な治療法が確立していない神経難病であるHAMの長期予後改善に結びつく，日本発の革新的な治療薬の創出につながり，HAMの治療にパラダイムシフトをもたらすことが期待される．

おわりに

HAMは長期にわたり障害を強いられる疾患で，患者の苦痛は大変深刻であり，一刻も早い有効な治療法の開発が切望されている．HAMのこれまでの研究により，感染細胞を標的とした薬剤開発はHAMの根本的な治療薬となることが期待されてきたが，これまで実現されなかった．ところが，近年の分子レベルでの病態解明やわが国の研究者によるバイオテクノロジー技術の進展などにより，その実現の可能性を探る臨床試験実施の機会が得られる段階にまで発展してきている．HAMは慢性炎症性疾患であるので，薬剤開発においては，安全性や長期忍容性などを

十分に配慮することが求められる．現状では，抗CCR4抗体製剤がHTLV-1感染細胞の劇的な減少を期待できる唯一の薬剤であるので，安全に治療可能な用量や用法などの決定に向け，慎重かつ綿密な臨床試験の実施を重ね，有用なエビデンスを蓄積していくことが重要と考える．

近年ではHAMの治療標的と成りうる細胞や分子の理解が進んできており，今後，新薬につながる成果がさらに得られることが期待される．また，ウイルス感染症と脊髄の慢性炎症の制御が，当面のHAM治療の達成すべき課題であるが，最近注目を集めている再生医療の応用も必要と考えられる．HAM患者は世界中に存在するが，先進国の中で患者数が多いのは日本のみであり，HAMの新薬開発研究におけるわが国の役割は大きい．

文　献

1) Osame M, Usuku K, Izumo S, et al. HTLV-I associated myelopathy, a new clinical entity. Lancet 1986 ; 1 : 1031.
2) Yamano Y, Sato T, Ando H, et al. [The current and future approaches to the treatment of HTLV-1-associated myelopathy/tropical spastic paraparesis (HAM/TSP)]. Nihon Rinsho 2012 ; 70 : 705. Japanese.
3) Nakagawa M, Izumo S, Ijichi S, et al. HTLV-I-associated myelopathy : analysis of 213 patients based on clinical features and laboratory findings. J Neurovirol 1995 ; 1 : 50.
4) Martin F, Fedina A, Youshya S, et al. A 15-year prospective longitudinal study of disease progression in patients with HTLV-1 associated myelopathy in the UK. J Neurol Neurosurg Psychiatry 2010 ; 81 : 1336.
5) Buyse M, Sargent DJ, Grothey A, et al. Biomarkers and surrogate end points–the challenge of statistical validation. Nat Rev Clin Oncol 2010 ; 7 : 309.
6) Olindo S, Lezin A, Cabre P, et al. HTLV-1 proviral load in peripheral blood mononuclear cells quantified in 100 HAM/TSP patients : a marker of disease progression. J Neurol Sci 2005 ; 237 : 53.
7) Takenouchi N, Yamano Y, Usuku K, et al. Usefulness of proviral load measurement for monitoring of disease activity in individual patients with human T-lymphotropic virus type I-associated myelopathy/tropical spastic paraparesis. J Neurovirol 2003 ; 9 : 29.
8) Sato T, Coler-Reilly A, Utsunomiya A, et al. CSF CXCL10, CXCL9, and Neopterin as Candidate Prognostic Biomarkers for HTLV-1-Associated Myelopathy/Tropical Spastic Paraparesis. PLOS Neglected Tropical Diseases 2013 ; 7 : e2479.
9) Zhou X, Bailey-Bucktrout SL, Jeker LT, et al. Instability of the transcription factor Foxp3 leads to the generation of pathogenic memory T cells in vivo. Nat Immunol 2009 ; 10 : 1000.
10) Yamano Y, Araya N, Sato T, et al. Abnormally high levels of virus-infected IFN-gamma$^+$ CCR4$^+$ CD4$^+$ CD25$^+$ T cells in a retrovirus-associated neuroinflammatory disorder. PLoS One 2009 ; 4 : e6517.
11) Yamano Y, Takenouchi N, Li HC, et al. Virus-induced dysfunction of CD4$^+$CD25$^+$T cells in patients with HTLV-I-associated neuroimmunological disease. J Clin Invest 2005 ; 115 : 1361.
12) Yamamoto-Taguchi N, Satou Y, Miyazato P, et al. HTLV-1 bZIP Factor Induces Inflammation through Labile Foxp3 Expression. PLoS Pathog 2013 ; 9 : e1003630.
13) Izumo S, Umehara F, Osame M. HTLV-I-associated myelopathy. Neuropathology 2000 ; 20 : S65.
14) Matsuoka E, Takenouchi N, Hashimoto K, et al. Perivascular T cells are infected with HTLV-I in the spinal cord lesions with HTLV-I-associated myelopathy/tropical spastic paraparesis : double staining of immunohistochemistry and polymerase chain reaction in situ hybridization. Acta Neuropathol 1998 ; 96 : 340.
15) Ando H, Sato T, Tomaru U, et al. Positive feedback loop via astrocytes causes chronic inflammation in virus-associated myelopathy. Brain 2013 ; 136 : 2876.
16) Taylor GP, Goon P, Furukawa Y, et al. Zidovudine plus lamivudine in Human T-Lymphotropic Virus type-I-associated myelopathy : a randomised trial. Retrovirology 2006 ; 3 : 63.
17) Macchi B, Balestrieri E, Ascolani A, et al. Suscepti-

bility of primary HTLV-1 isolates from patients with HTLV-1-associated myelopathy to reverse transcriptase inhibitors. Viruses 2011 ; 3 : 469.
18) Wattel E, Vartanian JP, Pannetier C, et al. Clonal expansion of human T-cell leukemia virus type I-infected cells in asymptomatic and symptomatic carriers without malignancy. J Virol 1995 ; 69 : 2863.
19) Cavrois M, Leclercq I, Gout O, et al. Persistent oligoclonal expansion of human T-cell leukemia virus type 1-infected circulating cells in patients with Tropical spastic paraparesis/HTLV-1 associated myelopathy. Oncogene 1998 ; 17 : 77.
20) 国際出願番号：PCT/JP2013/068296，発明者：山野嘉久．A THERAPEUTIC METHOD AND MEDICAMENT FOR HTLV-1 ASSOCIATED MYELOPATHY (HAM)．国際出願日：2013年7月3日．
21) Yamamoto K, Utsunomiya A, Tobinai K, et al. Phase I study of KW-0761, a defucosylated humanized anti-CCR4 antibody, in relapsed patients with adult T-cell leukemia-lymphoma and peripheral T-cell lymphoma. J Clin Oncol 2010 ; 28 : 1591.
22) Ishida T, Joh T, Uike N, et al. Defucosylated anti-CCR4 monoclonal antibody (KW-0761) for relapsed adult T-cell leukemia-lymphoma : a multicenter phase II study. J Clin Oncol 2012 ; 30 : 837.

* * *

Cancer Science
Japanese Cancer Association JCA
Open Access

Epigenetic deregulation of *Ellis Van Creveld* confers robust Hedgehog signaling in adult T-cell leukemia

Ryutaro Takahashi,[1,6] Makoto Yamagishi,[1,6] Kazumi Nakano,[1] Toshiko Yamochi,[2] Tadanori Yamochi,[1] Dai Fujikawa,[1] Makoto Nakashima,[1] Yuetsu Tanaka,[3] Kaoru Uchimaru,[4] Atae Utsunomiya[5] and Toshiki Watanabe[1]

[1]Graduate School of Frontier Sciences, The University of Tokyo, Tokyo; [2]Department of Pathology, Showa University School of Medicine, Tokyo; [3]Department of Immunology, Graduate School of Medicine, University of the Ryukyus, Okinawa; [4]Institute of Medical Science, The University of Tokyo, Tokyo; [5]Department of Hematology, Imamura Bun-in Hospital, Kagoshima, Japan

Key words

ATL, epigenetics, EVC, Hedgehog, HTLV-1

Correspondence

Toshiki Watanabe, Laboratory of Tumor Cell Biology, Department of Medical Genome Sciences, Graduate School of Frontier Sciences, The University of Tokyo, 4-6-1 Shirokanedai, Minato-ku, Tokyo 108-8639, Japan.
Tel: +81-3-5449-5298; Fax: +81-3-5449-5418;
E-mail: tnabe@ims.u-tokyo.ac.jp

[6]These authors contributed equally to this study.

Funding information

JSPS KAKENHI (24790436). (23390250). MEXT KAKENHI (221S0001). Ministry of Health, Labour and Welfare H24-Third Term Cancer-004 Uehara Memorial Foundation.

Received April 14, 2014; Revised June 20, 2014; Accepted July 1, 2014

Cancer Sci **105** (2014) 1160–1169

doi: 10.1111/cas.12480

One of the hallmarks of cancer, global gene expression alteration, is closely associated with the development and malignant characteristics associated with adult T-cell leukemia (ATL) as well as other cancers. Here, we show that aberrant overexpression of the *Ellis Van Creveld* (EVC) family is responsible for cellular Hedgehog (HH) activation, which provides the pro-survival ability of ATL cells. Using microarray, quantitative RT-PCR and immunohistochemistry we have demonstrated that EVC is significantly upregulated in ATL and human T-cell leukemia virus type I (HTLV-1)-infected cells. Epigenetic marks, including histone H3 acetylation and Lys4 trimethylation, are specifically accumulated at the *EVC* locus in ATL samples. The HTLV-1 Tax participates in the coordination of EVC expression in an epigenetic fashion. The treatment of shRNA targeting EVC, as well as the transcription factors for HH signaling, diminishes the HH activation and leads to apoptotic death in ATL cell lines. We also showed that a HH signaling inhibitor, GANT61, induces strong apoptosis in the established ATL cell lines and patient-derived primary ATL cells. Therefore, our data indicate that HH activation is involved in the regulation of leukemic cell survival. The epigenetically deregulated EVC appears to play an important role for HH activation. The possible use of EVC as a specific cell marker and a novel drug target for HTLV-1-infected T-cells is implicated by these findings. The HH inhibitors are suggested as drug candidates for ATL therapy. Our findings also suggest chromatin rearrangement associated with active histone markers in ATL.

Adult T-cell leukemia (ATL) is a malignant T-cell disorder caused by infection with a human retrovirus, human T-cell leukemia virus type I (HTLV-1).[1–3] The prognosis of aggressive types of ATL is poor.[4] At present, ATL is an intractable disease in human beings. To prevent the development of ATL and the poor prognosis that is associated with it, the development of effective therapies based on the molecular characteristics is needed.

To explore effective drugs, precise understanding of the molecular mechanism of ATL pathogenesis is essential. We have previously reported that genetic and epigenetic imbalances and following aberrant gene expressions are the main framework for ATL tumor cells.[5,6] In addition, the involvement of systemic downregulation of cellular microRNA has been implicated in the leukemogenesis of ATL. So far, several host cellular signaling abnormalities induced by HTLV-1 Tax in the early phase of infection[6–8] and the aberrant activation of nuclear factor-kappa B (NF-κB) contribute to ATL leukemogenesis.[9,10] Although other several molecular deregulations have been suggested in ATL, we have not completely covered the landscape of signaling networks in ATL.

Recently, Hedgehog (HH) signaling has been reported as an oncogenic pathway in many types of cancers.[11,12] Constitutive HH activation leads to the overproliferation or survival of several cancer cells, such as basal cell carcinoma or B-cell lymphomas.[13–15] There are some HH inhibitors under clinical trial as drug candidates against those cancers.[16]

In the present study, using ATL patient samples and some ATL models, we found two specific gene overproductions in ATL, *Ellis Van Creveld syndrome 1* (*EVC1*) and *EVC2*, which belong to the EVC family of genes that are implicated in HH regulation.[17–19] We demonstrated that epigenetically upregulated EVC was associated with cellular HH activity. *EVC* and other regulatory factors for HH signaling were responsible for the survival of ATL cell lines and also primary ATL samples. Direct evidence from the ATL samples revealed that universal epigenetic marks associated with actively transcribed genes were rearranged in the leukemic cells. These findings may shed light on the abnormal gene expression signature and leukemic cell traits observed in ATL.

Materials and Methods

Patient samples. The primary peripheral blood mononuclear cells (PBMC) from ATL patients and healthy volunteers were a part of those collected with informed consent as a collaborative project of the Joint Study on Prognostic Factors of ATL Development (JSPFAD). The project was approved by the University

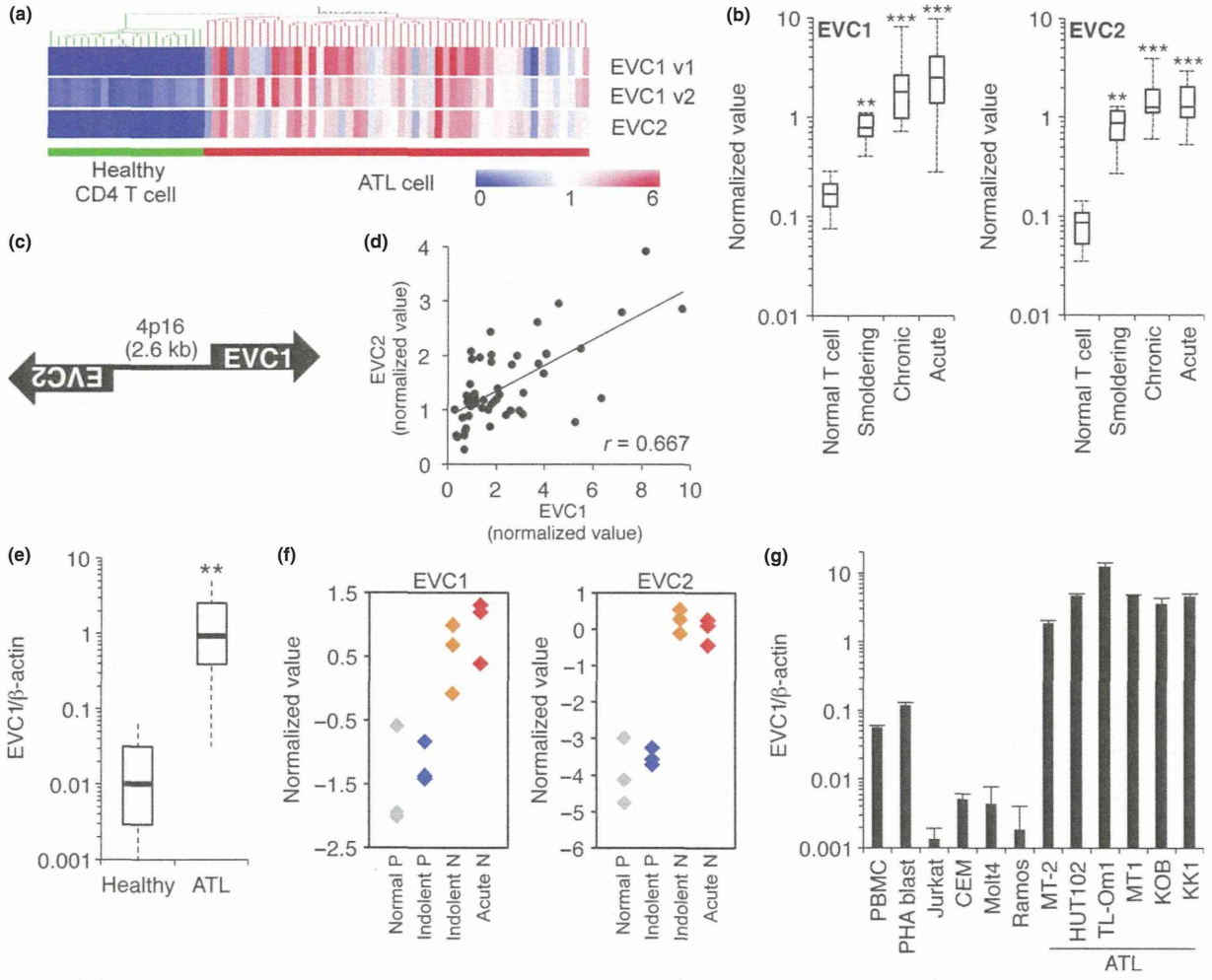

Fig. 1. *EVC* overexpression in ATL. (a, b) Microarray heatmap (a) and box plot (b) of *EVC*. $^{**}P < 0.01$. $^{***}P < 0.001$. (c) Schematic illustration of locus encoding *EVC1/2*. (d) Individual expression values ($n = 52$) between *EVC1* and *EVC2*. (e) *EVC1* mRNA level in ATL patient PBMC (total, $n = 11$; acute, $n = 7$; chronic, $n = 4$) and in CD4+ T cells from healthy donors ($n = 6$) evaluated using quantitative RT-PCR (qRT-PCR). $^{**}P < 0.01$. (f) *EVC1* and *EVC2* levels in CADM1 versus CD7 plot subpopulations. Normal P, CD4+/CADM1−/CD7+ T cells from healthy donors; Indolent P, CD4+/CADM1−/CD7+ from indolent ATL patients; Indolent N, CD4+/CADM1+/CD7− from indolent ATL patients; Acute N, CD4+/CADM1+/CD7− from acute ATL patients. The gene expression microarray dataset is available in Kobayashi *et al.*[25] (g) *EVC1* levels in various cell lines examined using qRT-PCR ($n = 3$, mean ± SD).

of Tokyo and Showa University research ethics committees. The PBMC were isolated using Ficoll separation and maintained in RPMI1640 (Invitrogen, Carlsbad, CA, USA) supplemented with 1% of self-serum and antibiotics (Invitrogen). Clinical information is shown in the Supporting Information Methods.

Microarray analysis. Gene expression profiling of ATL patient samples and normal CD4+ T cells has been performed previously.[5] The coordinate has been deposited in the Gene Expression Omnibus database (GSE33615).

Cell culture. The HTLV-1-infected cell lines MT-2 and HUT102, ATL-derived cells MT-1 and TL-Om1, and other leukemic cell lines were cultured in RPMI1640 with 10% FCS. ATL-derived KOB and KK1 were cultured in RPMI1640 with 10% FCS and 10 ng/mL recombinant human IL-2 (R&D Systems, Minneapolis, MN, USA). The 293T cell was cultured in DMEM with 10% FCS. All cell lines were cultured at 37°C, with 5% CO_2.

Plasmids and HH activity analysis. Tax-encoding plasmids have been described previously.[20] *EVC1* cDNA was amplified as two fragments from the human cDNA library. Cellular HH activity was evaluated using a dual-luciferase assay (Promega, Madison, WI, USA).[21] Briefly, 7 × GLI binding site (GACACCCA)-luciferase plasmid and control RSV-Renilla plasmid were co-transfected into target cells using Lipofectamine2000 (Invitrogen). At 24 h post-transfection, the cells were collected and analyzed using a dual-luciferase assay.

Quantitative RT-PCR. Procedures for RNA isolation and RT-PCR have been described previously.[5] Primer sets for quantitative RT-PCR (qRT-PCR) are provided in the Supporting Information Methods.

Epigenetic analyses. Bisulfite treatment was conducted using a MethylEasy Xceed Rapid DNA Bisulphite Modification kit (Human Genetic Signatures, NSW, Australia). For evaluating histone covalent modifications, a chromatin immunoprecipita-

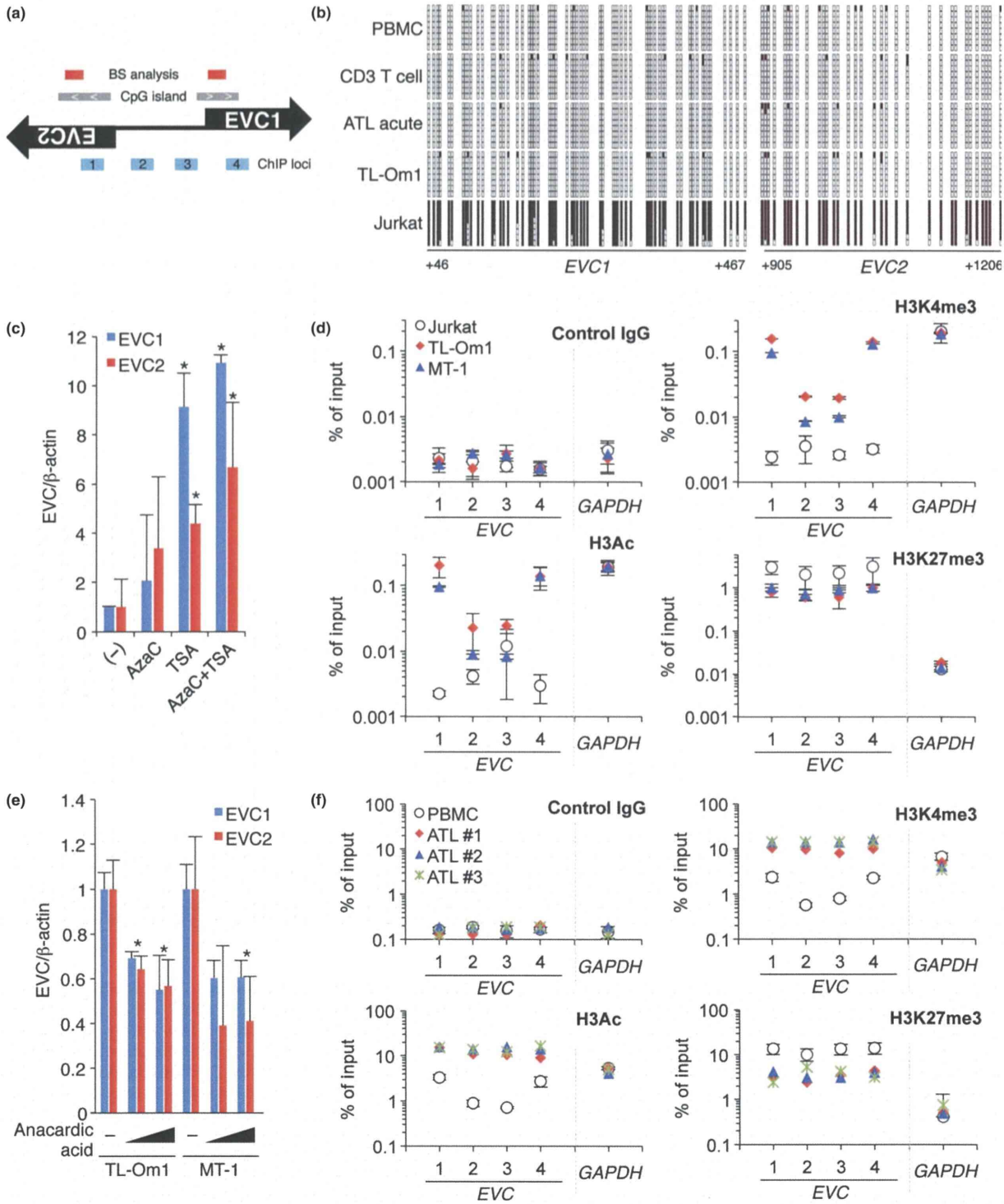

Fig. 2. Epigenetic reprogramming in the *EVC* locus. (a) Schematic of CpG islands and chromatin immunoprecipitation (ChIP) loci. (b) Results of bisulfite sequencing (+46 to +466 from *EVC1* transcription start site [TSS]; +905 to +1206 from *EVC2* TSS). The black and empty boxes represent methylated and unmethylated CpG, respectively. (c) *EVC* RNA levels in Jurkat cells in the presence or absence of epigenetic drugs ($n = 3$, mean ± SD). $^*P < 0.05$. (d) Histone covalent modifications at *EVC* and *GAPDH* loci in three cell lines were analyzed using PCR-based ChIP assay with specific antibodies. Positions of primer sets for the real-time PCR are indicated in (a). Enrichment values relative to input samples are plotted. (e) TL-Om1 and MT-1 cells were treated with 1 or 5 μM of anacardic acid for 48 h and the *EVC* mRNA level was then analyzed ($n = 3$, mean ± SD). $^*P < 0.05$. (f) Epigenetic changes in primary ATL samples. Three independent clinical samples were compared with normal PBMC ($n = 3$, mean ± SD).

tion (ChIP) assay was conducted as described previously.[5,22] Anti-H3K4me3 (#9751S; Cell Signaling, Danvers, MA, USA), anti-AcH3 (#06-599; Millipore, Billerica, MA, USA), anti-H3K27me3 (#39155; Active Motif, Carlsbad, CA, USA) and control IgG (I5381; SIGMA, St. Louis, MO, USA) were used for ChIP. Primers for the qPCR are provided in the Supporting Information Methods.

Immunohistochemistry. For preparation of the paraffin block of 293T cells, the cells were fixed in 20% of formalin/PBS for 24 h. After removing the formalin, alcohol dehydration and paraffin permeation were done using Tissue-Tek VIP5Jr (Sakura, Alphen aan den Rijn, The Netherlands). Paraffin blocks were sectioned at 3-μm thickness. The sections were then transferred to coating slide glasses (Muto pure chemicals, Bunkyo-ku, Tokyo, Japan). After paraffin removal, the paraffin sections of the 293T and ATL cells were treated with 3% H_2O_2. Antigen-retrieval treatment was done using Histofine antigen retrieval solution pH9 (Nichirei, Chuo-Ku, Tokyo, Japan) for 20 min under microwave radiation. After reaction with the first antibody, anti-EVC antibody (HPA008703, 1:400; SIGMA), and the second antibody (K5027, ENVISION Kit/HRP [DAB]; Dako, Bunkyo-ku, Tokyo, Japan), the sections were colored using ENVISION Kit/HRP [DAB] DAB+ (K3468; DAKO). Finally, the sections were stained with hematoxylin.

Lentivirus construction and production. Detailed procedures for lentivirus production have been described previously.[5] Briefly, replication-defective, self-inactivating lentivirus vectors were used.[23,24] shRNA were cloned into a CS-H1-EVBsd. High-titer viral solutions prepared using a centrifugation-based concentration were transduced into ATL cell lines using the spinoculation method. The transduced cells were

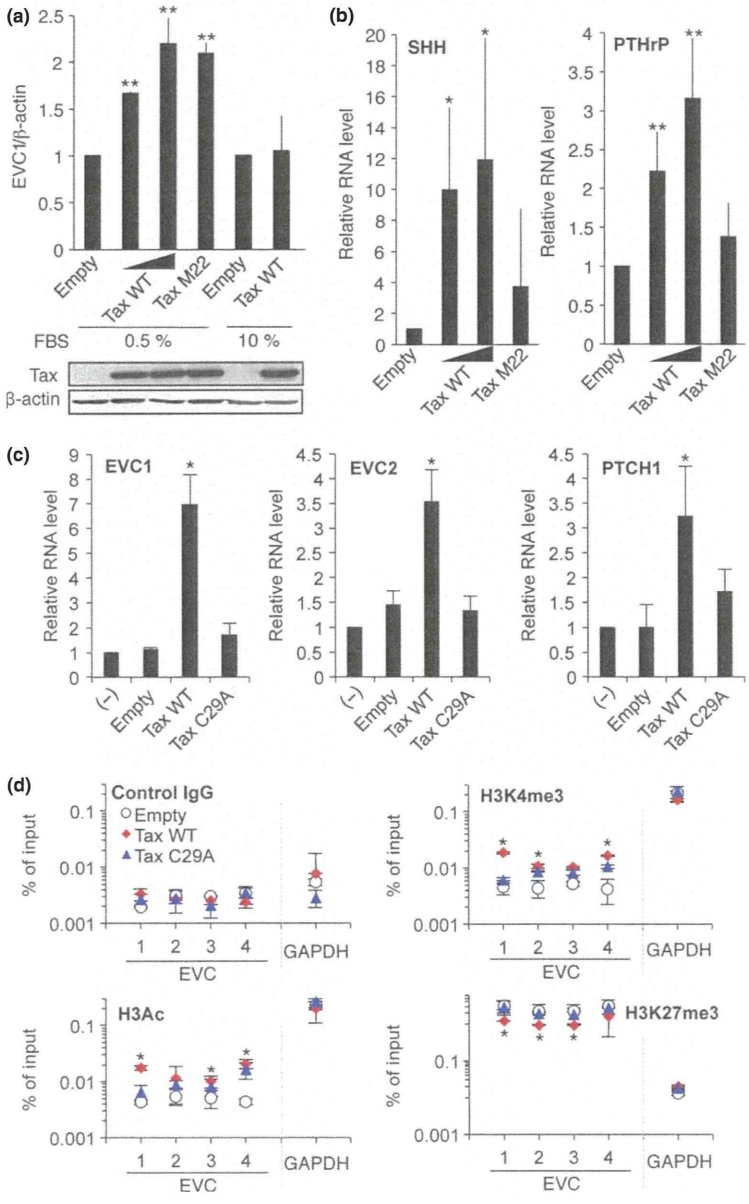

Fig. 3. Role of Tax in *EVC* regulation. (a) *EVC1* RNA levels are affected by Tax. The 293T cells in different FBS condition were transfected with the indicated plasmids. Relative *EVC1* levels were evaluated using quantitative RT-PCR (qRT-PCR) (top panel, $n = 3$, mean ± SD). $^{**}P < 0.01$. Tax expression was confir-med using western blotting with an anti-Tax antibody (Lt-4) (bottom panel). (b) Levels of *SHH* and *PTHrP* in the presence or absence of Tax ($n = 3$, mean ± SD). $^{*}P < 0.05$. $^{**}P < 0.01$. (c) *EVC* and *PTCH1* levels in Jurkat cells expressing Tax ($n = 3$, mean ± SD). $^{*}P < 0.05$. (d) Tax-mediated epigenetic changes. Histone modifications at *EVC* and *GAPDH* loci in Tax-expressing Jurkat cells were analyzed using a ChIP assay. $^{*}P < 0.05$ (Tax WT *vs* Empty). Primer positions are shown in Figure 2(a).

further selected by blastcidin and used within 14 days. shRNA sequences are described in the Supporting Information Methods.

Cell viability and apoptosis analyses. For the cell proliferation assay, 5000 cells were plated in a 96-well flat bottom plate with RPMI1640 medium supplemented with 1% FCS. After 1–3 days culture, cell numbers were evaluated using Cell Counting kit-8 (Dojindo, Kumamoto, Japan). The apoptosis cell was determined using PE Annexin V/7-AAD stainings (BD Pharmingen, San Jose, CA, USA). Detection of apoptotic cells was performed using FACSCalibur (Becton, Dickinson, Franklin Lakes, NJ, USA). Primary ATL cells were defined using sequential gating based on a Forward scatter/Side Scatter (FSC/SSC) pattern and a CD4-positive population (anti-CD4-FITC; BD Pharmingen). Collected data were analyzed using FlowJo software (Tree Star, Ashland, OR, USA).

Results

Epigenetic abnormalities in *EVC* regulation in ATL. We have determined the gene expression signature of ATL tumor cells by conducting massive microarrays.[5] The gene expression profiles from 52 ATL patients and 21 healthy donors identified a large number of specific gene upregulations in ATL cells. Among these, the genes encoding EVC1 and EVC2 were strikingly overexpressed in ATL patient samples, which had a relationship to disease progression (Fig. 1a,b). These genes are located in an identical chromosome *4p16*, under a bi-directional promoter (Fig. 1c), and their expressions have shown a strong positive correlation (Fig. 1d). The qRT-PCR revealed that the median of the *EVC1* mRNA level in ATL was 90.9-fold higher than that of normal CD4+ T-cells (Fig. 1e). Specificity of tumor-associated EVC expression was confirmed using the dataset from CADM1 versus CD7 plot subpopulation samples.[25] CADM1 expression and CD7 loss have recently been identified as highly sensitive molecular markers of HTLV-1-infected cells. *EVC1* and *EVC2* were significantly expressed in the CADM1+/CD7− tumorous population (Fig. 1f). The HTLV-1-infected and ATL-derived cells showed higher levels of *EVC1* mRNA compared with those in other leukemia and lymphoma cell lines and those of healthy PBMC (Fig. 1g). The MT-2 and HUT102 cells, which highly express HTLV-1 genes, showed high *EVC1* mRNA levels similar to those in ATL-derived cells.

Looking at the tumor-associated epigenetic reprogramming that was frequently observed in ATL,[5,6] we analyzed the epigenetic status of the *EVC* locus to clarify the possible

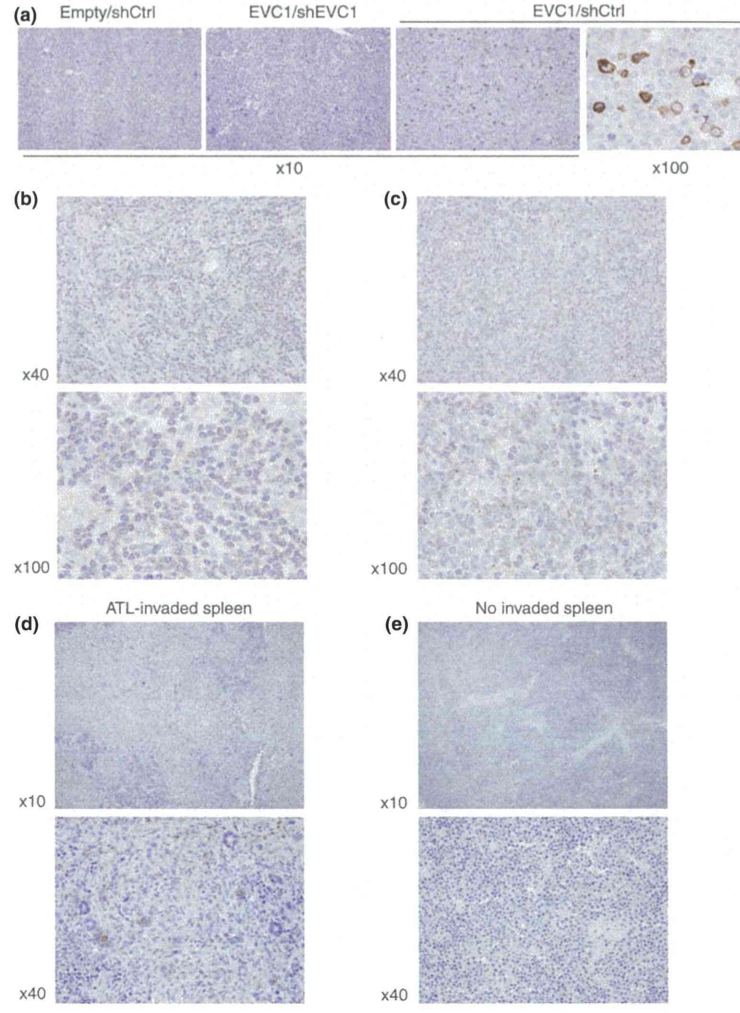

Fig. 4. EVC1 expression in ATL cells. (a–e) Immunohistochemistry-based EVC1 protein detection in paraffin-embedded samples: 293T transfected with the indicated plasmids (a), primary ATL lymph node (b, c, representative data are shown) and spleen from mice engrafted with primary ATL cells (d, tumor invasive, $n = 3$; e, non-invasive). These samples were stained with anti-EVC1 antibody and hematoxylin.

involvement of epigenetic variation in *EVC* deregulation. There were two typical CpG islands in the *EVC* locus whose transcription may be tightly regulated by the gain of CpG methylation (Fig. 2a). However, bisulfite sequencing revealed that DNA methylation was not acquired in normal lymphocytes, as well as in the primary ATL sample (Fig. 2b). CpG hypermethylation within the *EVC* locus was found only in Jurkat cells where the *EVC* expression was nearly undetectable (Fig. 1g). Instead, treatment with epigenetic drugs, particularly a histone deacetylase (HDAC) inhibitor tricostatin A (TSA), reactivated the *EVC* transcription in Jurkat cells, suggesting that histone modifications such as acetylation were involved in *EVC* regulation (Fig. 2c). To further address the epigenetic implication, we performed ChIP assays to assess the possible contribution of histone modification in *EVC* upregulation. The ATL cell lines showed significant accumulation (log-scale) of histone H3 acetylation (H3Ac) and H3K4 trimethylation (H3K4me3), which have been recognized generally as positive transcription marks around the transcription start site region of both *EVC1* and *EVC2* (Fig. 2d). Treatment with a pan-histone acetylase inhibitor, anacardic acid, reduced *EVC* transcription in ATL cell lines (Fig. 2e). Interestingly, H3K27me3, which has been implicated as a poor prognostic marker in ATL,[5,26] was decreased at the *EVC* locus in ATL cells. We confirmed directly the epigenetic reprogramming at the *EVC* locus in primary ATL samples (Fig. 2f). In summary, it appeared that the acquisition of active histone modifications and the reciprocal disappearance of H3K27me3 contributed to aberrant EVC transcription.

Role of HTLV-1 Tax in *EVC* transcription. Next we addressed whether Tax could participate in the deregulated *EVC1* transcription. Although Tax expression did not influence the *EVC1* mRNA levels in 293T cells at complete growth conditions, Tax activated *EVC1* transcription in a dose-dependent manner in serum-starved conditions (Fig. 3a). A NF-κB activation-defected Tax mutant, M22,[27] showed similar *EVC1* induction, suggesting that *EVC1* transcriptional activation was independent from NF-κB activation. Indeed, the pharmacological inhibition of NF-κB activity failed to prevent *EVC* transcription in ATL cell lines (data not shown). Meanwhile, Tax induced transcription of *Sonic hedgehog* (*Shh*), which encodes the HH activation ligand, in a NF-κB-dependent manner (Fig. 3b). The experimental condition was validated by the evaluation of *PTHrP*, which has been known to be a Tax and NF-κB-targeted gene. HTLV-1 *HBZ* did not affect *EVC* transcription (Supporting Information Fig. S1).

We examined the possible relationship between Tax and histone modifications. For this purpose, we established lentiviral vectors inducing stable Tax expression in Jurkat cells. More than 80% of transduction efficiencies were achieved in all tested cells. Tax induced transcription of *EVC1* and *EVC2*, as well as the HH target gene *PTCH1* (Fig. 3c). Interestingly, the Tax C29A mutant, which was unable to localize in the nucleus,[28] failed to induce *EVC*, suggesting that *EVC* induction was directly caused by the nuclear-localized Tax. A ChIP assay revealed that the Tax wild type, but not the C29A mutant, directly accumulated H3K4me3 and H3Ac in the *EVC* locus (Fig. 3d). Thus, Tax appeared to, at least partially, induce *EVC* expression through epigenetic reprogramming.

EVC1 expression in primary ATL cell. We performed immunohistochemistry (IHC) with a commercially available antibody that recognized EVC1. First, we stained paraffin-embedded 293T cells transduced with the EVC1-expressing plasmid to test the antibody specificity. Strong positivity was detected in the plasmid-transduced sample but not in samples with untreated or concomitantly treated with shRNA targeting *EVC1* (Fig. 4a). Using this antibody we investigated EVC1 expression in several aggressive ATL cases. Most ATL cases showed stable EVC1 positivity (7/8, 87.5%; two representatives in Fig. 4b,c). We noted that all EVC1-positive cells were dysplastic. Furthermore, EVC1 expression was clearly detected in a mouse ATL model that was established using xenotrans-

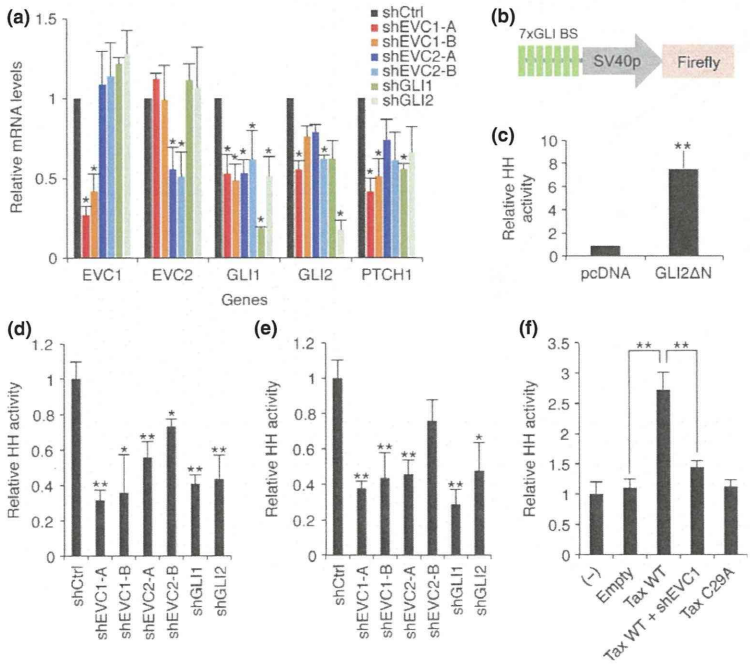

Fig. 5. EVC supports Hedgehog (HH) activity. (a) Relative RNA levels in shRNA-expressing TL-Om1 cells ($n = 3$, mean ± SD). $^{*}P < 0.05$. (b) Luciferase reporter plasmid containing 7 × sequential GLI-binding sites. (c) GLI2ΔN activa-ted HH activity ($n = 3$, mean ± SD). $^{**}P < 0.01$. (d–f) Hedgehog activity in various shRNA-expressing TL-Om1 (d), MT-2 (e) and Tax and shEVC1-expressing Jurkat (f) ($n = 3$–4, mean ± SD). $^{*}P < 0.05$. $^{**}P < 0.01$.

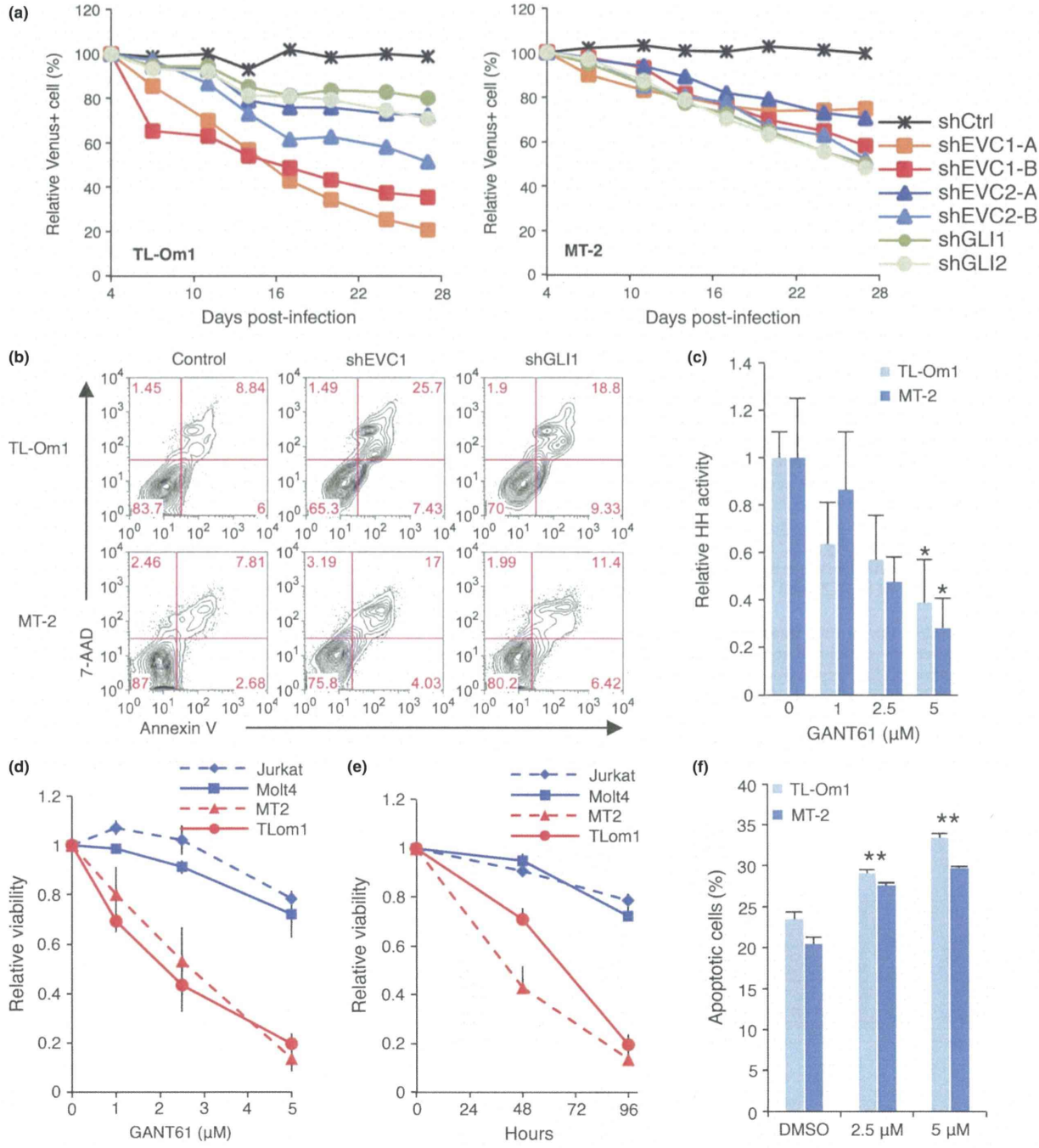

Fig. 6. Hedgehog (HH)-dependent ATL cell survival. (a) Time course of the abundance of Venus+ TL-Om1 (left) and MT-2 (right) infected with lentiviral vector expressing control shRNA (shCtrl), either of two shRNA targeting EVC1 and EVC2, or shRNA targeting GLI1 and GLI2, then cultured for 27 days together with uninfected cells. Data are representative of three independent experiments. Results are presented relative to those of cells at 4 days post-infection. (b) shRNA-mediated apoptosis induction. shRNA-expressing cells were cultured in 1% FBS for 72 h. The apoptotic pattern was defined by gating with Venus+ and Annexin V/7-AAD ($n = 3$, representative data). (c) GANT61 inhibited HH activity in ATL cells ($n = 3$, mean ± SD). *$P < 0.05$. (d–e) GANT61 reduced ATL cell viability ($n = 3$, mean ± SD). The cells were treated with the indicated concentrations of GANT61 for 96 h (d) or with 5 μM of GANT61 for the indicated time periods (e). Cells were maintained in 1% FCS. (f) GANT61-dependent apoptosis analyzed using Annexin V/7-AAD staining ($n = 3$, mean ± SD). **$P < 0.01$.

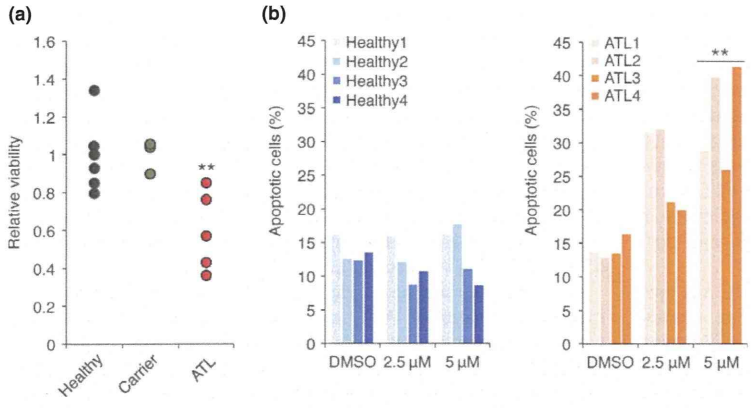

Fig. 7. GANT61 treatment reduced cell viabilities of primary ATL samples. (a) Effect of GANT61 in primary PBMC samples. The PBMC from healthy donors (n = 7), asymptomatic carriers (n = 3) and ATL patients (n = 5) were exposed in 5 μM of GANT61 for 72 h. Cells were maintained in media with 1% self-serum. $^{**}P < 0.01$. (b) GANT61-dependent apoptosis in ATL samples. The PBMC from healthy donors (n = 4) and ATL patients (n = 4) were treated with 5 μM of GANT61 for 72 h. Graphs show percentiles of apoptotic population in CD4+ cells $^{**}P < 0.01$.

plantation of primary tumor cells derived from an ATL patient. The lymphoma cells specifically expressed EVC1 (Fig. 4d,e). Taken together, EVC1 protein was definitely expressed in ATL cells.

EVC in HH activation. The EVC family has been implicated in HH signaling.[18,19] We performed the knockdown of EVC in TL-Om1 and MT-2 cells, which all highly expressed EVC (Fig. 1g). Specific knockdown was accomplished using lentivirus harboring specific and previously validated shRNA against EVC1, EVC2 or GLI transcription factors in the HH cascade. The qRT-PCR revealed the knockdown efficiency and also the HH activity as the RNA levels of *PTCH1* and *GLI1* were well-established HH activity markers.[29] The EVC depletion resulted in reduction of *PTCH1* and *GLI1* mRNA levels (Fig. 5a). Next we established a luciferase reporter containing 7 × sequential GLI-binding sites (Fig. 5b), which strongly responded against GLI2ΔN, a constitutive active form of GLI2[12] (Fig. 5c). As expected, the knockdown of EVC1 and EVC2 represented diminished HH activity in TL-Om1 and MT-2 cells (Fig. 5d,e). In addition, Tax activated the HH signal in Jurkat cells (Fig. 5f). Knockdown of EVC1 cancelled Tax-directed HH activation, suggesting that Tax affects HH signaling through, at least partially, EVC induction epigenetically.

EVC-dependent cell survival in ATL. Aberrant activation of HH provides cell survival ability in myeloma and lymphoma.[14,15] We found that different shRNA targeting EVC and GLI caused a progressive depletion of Venus+ cells (Fig. 6a). Knockdown of EVC1 or EVC2 attenuated ATL cell proliferation (Fig. S2). The growth defect was associated with a substantial decrease in the expression of targeted genes (Fig. 5). We then measured the apoptotic status by staining Annexin V/7-AAD. Specific analyses within the knocked down cells were achieved by gating with Venus fluorescence. At complete growth condition, slight but steady apoptosis was induced by EVC1 knockdown in MT-2 and TL-Om1 cells (data not shown). Furthermore, strong apoptosis was observed in EVC1-depleted cells at low FCS condition (Fig. 6b). This cell death appeared to be due to HH inactivation because GLI1-knocked down cells showed similar results.

Specific killing of ATL cell by GANT61. GANT61 is a cell-permeable hexahydropyrimidine compound, which has been shown to be a well-established inhibitor of GLI-mediated gene transactivation.[29] GANT61 treatment successfully reduced GLI binding to the target sequence (Fig. 6c). In that condition, MT-2 and TL-Om1 cells showed remarkable reduction of cell viability by GANT61 treatment in dose- and time-dependent manners (Fig. 6d,e), which may be caused by apoptosis (Fig. 6f).

Finally, we evaluated the pharmacological activity of GANT61 on primary ATL samples. Although GANT61 did not show a clear effect on PBMC derived from healthy donors and HTLV-1 carriers, its treatment specifically reduced the viability of ATL samples significantly (Fig. 7a). Flow cytometry demonstrated that GANT61 specifically killed CD4+ leukemic cells from ATL patients via apoptosis induction (Fig. 7b).

Discussion

A large number of efforts have collectively concluded that aberrant gene expression patterns contribute to the malignant characteristics in ATL and other neoplastic cells. In the present study, based on the careful analyses of patient samples, we have demonstrated that *EVC* is drastically overexpressed in mRNA and its protein can be specifically detected in ATL cells in contrast to normal CD4+ T-cells. To the best of our knowledge, this is the first report regarding EVC expression and function in lymphocytes. The results of the microarray indicate that *EVC* expression appears to be induced in accordance with disease progression. EVC1 protein expression is observed in dysplastic ATL cells derived from patients and a xenotransplantation model. Because the EVC family may be membrane-associated proteins (Fig. 4),[30] the present study provides us with the possibility that EVC expressions might be useful cell markers of HTLV-1-infected T-cells for future clinical purposes.

The EVC family has been identified initially as the responsible genes for one morphogenic disorder, Ellis van Creveld syndrome; it is also believed to play a role in the determination of body-axis or morphogenesis by usually bearing one step of the HH signaling pathway.[12,17–19] Knockout studies have demonstrated that EVC1 and EVC2 cooperatively act as positive modulators of the HH pathway in mouse fibroblasts and chondrocytes. However, abnormal EVC upregulation has not been reported in any cancers; whether the HH pathway is sensitive to cellular dynamism of EVC has not been elucidated as yet. Herein, we demonstrated that overexpression of EVC can be linked to HH activity in T cells for the first time. In addition, several experimental results, including the knockdown assay and GANT61 treatment, suggest totally that the HH pathway was activated in ATL, which in turn contributed to ATL cell survival. Further study will be required for mechanistic insights on how EVC activates HH in T cells.

Further investigation uncovered that transcription from the *EVC* locus was coordinated by epigenetic alteration. In particular, the lymphoma-associated H3Ac and H3K4me3 accumulations appeared to dominate EVC upregulation. Direct evidence from patient samples supported the epigenetic reprogramming, including previously unappreciated H3K4me3 rearrangements, conferring robust EVC expression. Interestingly, repressive histone mark H3K27me3 was mutually reduced at the *EVC* locus in the ATL samples, suggesting that cooperative regulation in this bivalent domain may define the EVC expression and possibly HH activity.

HTLV-1 Tax was involved in the regulation of EVC via epigenetic regulation. Nuclear localization-deficient Tax mutant was unable to induce EVC expression, implying that Tax may participate directly in determination of chromatin architecture. Indeed, lentiviral expression of Tax partially increased active histone modifications, which in turn activated HH signaling. Previously, we and others have reported that Tax physically binds with histone modifying factors, including HDAC,[31] SUV39H1[32] and SMYD3.[20] Interplay between Tax and epigenetic rearrangement may be closely involved in the progression of HTLV-1-infected cells to leukemic cells. Meanwhile, other ATL-specific epigenetic events including significant modifications on histone acetylation, H3K4me3 and H3K27me3 clearly dominate stable EVC expression. The alteration of the epigenetic landscape by Tax and other molecular mechanisms such as expression changes of epigenetic modifiers will be elucidated by comprehensive analysis such as a genome-wide ChIP analysis.

In the context of molecular targeting, a new possibility for the HH inhibitor was suggested. Recently, aberrant HH activation and its contribution to cell survival and the cell cycle have been reported in various cancer cells.[11,12] In agreement with other tumors where HH is active, we found that ATL was sensitive against GANT61. This compound can inhibit HH signaling by preventing DNA binding of the GLI family and has few impacts on the viability of healthy CD4+ T cells. We note that we could not confirm the EVC-directed upregulation of common HH target genes such as *Cyclin D1* and *Bcl-2* in ATL models (data not shown). Given that the HH pathway regulates transcription of many genes important for cell fate and many inhibitors against HH cascade have been developed,[16] our findings suggest that pharmacological drugs that can inhibit the HH pathway may be feasible for ATL treatment. Identification of ATL-specific HH target genes will help understanding of the HH roles in survival capability.

In summary, we have identified EVC overexpression as a specific character of ATL and HTLV-1-infected T cells. We have demonstrated the molecular mechanism that overexpressed EVC1 contributes to ATL cell survival. Considering aberrant gene expression associated with cancers, the emerging relationship between epigenetic regulation and the HH pathway provides us with conceptual advance in understanding the broad-acting oncogenic signaling.

Acknowledgments

The authors thank Dr M. Iwanaga and Ms T. Akashi for support and maintenance of JSPFAD and Mr Y. Sasaki for experimental support of the IHC study. The authors also thank Drs H. Miyoshi and A. Miyawaki for providing the Venus-encoding lentivirus vectors and Dr S. Okada for providing the NOJ mice. This work is supported by JSPS KAKENHI Grant Numbers 24790436 (M.Y.) and 23390250 (T.W.), MEXT KAKENHI Grant Number 221S0001 (T.W.), Grant-in-Aid from the Ministry of Health, Labour and Welfare H24-Third Term Cancer-004 (T.W.), and a grant from the Uehara Memorial Foundation (M.Y.).

Disclosure Statement

The authors have no conflict of interest.

References

1 Uchiyama T, Yodoi J, Sagawa K, Takatsuki K, Uchino H. Adult T-cell leukemia: clinical and hematologic features of 16 cases. *Blood* 1977; **50**: 481–92.
2 Poiesz BJ, Ruscetti FW, Gazdar AF, Bunn PA, Minna JD, Gallo RC. Detection and isolation of type C retrovirus particles from fresh and cultured lymphocytes of a patient with cutaneous T-cell lymphoma. *Proc Natl Acad Sci USA* 1980; **77**: 7415–9.
3 Yoshida M, Miyoshi I, Hinuma Y. Isolation and characterization of retrovirus from cell lines of human adult T cell leukemia and its implication in the disease. *Proc Natl Acad Sci USA* 1982; **79**: 2031–5.
4 Tsukasaki K, Utsunomiya A, Fukuda H *et al.* VCAP-AMP-VECP compared with biweekly CHOP for adult T-cell leukemia–lymphoma: Japan Clinical Oncology Group Study JCOG9801. *J Clin Oncol* 2007; **25**: 5458–64.
5 Yamagishi M, Nakano K, Miyake A *et al.* Polycomb-mediated loss of miR-31 activates NIK-dependent NF-κB pathway in adult T cell leukemia and other cancers. *Cancer Cell* 2012; **21**: 121–35.
6 Yamagishi M, Watanabe T. Molecular hallmarks of adult T cell leukemia. *Front Microbiol* 2012; **3**: 334.
7 Grassmann R, Aboud M, Jeang KT. Molecular mechanisms of cellular transformation by HTLV-1 Tax. *Oncogene* 2005; **24**: 5976–85.
8 Hall WW, Fujii M. Deregulation of cell-signaling pathways in HTLV-1 infection. *Oncogene* 2005; **24**: 5965–75.
9 Mori N, Fujii M, Ikeda S *et al.* Constitutive activation of NF-kappaB in primary adult T-cell leukemia cells. *Blood* 1999; **93**: 2360–8.
10 Watanabe M, Ohsugi T, Shoda M *et al.* Dual targeting of transformed and untransformed HTLV-1-infected T cells by DHMEQ, a potent and selective inhibitor of NF-kappaB, as a strategy for chemoprevention and therapy of adult T-cell leukemia. *Blood* 2005; **106**: 2462–71.
11 Low JA, de Sauvage FJ. Clinical experience with Hedgehog pathway inhibitors. *J Clin Oncol* 2010; **28**: 5321–6.
12 Briscoe J, Thérond PP. The mechanisms of Hedgehog signalling and its roles in development and disease. *Nat Rev Mol Cell Biol* 2013; **14**: 416–29.
13 Johnson RL, Rothman AL, Xie J *et al.* Human homolog of patched, a candidate gene for the basal cell nevus syndrome. *Science* 1996; **272**: 1668–71.
14 Dierks C, Grbic J, Zirlik K *et al.* Essential role of stromally induced hedgehog signaling in B-cell malignancies. *Nat Med* 2007; **13**: 944–51.
15 Singh RR, Kim JE, Davuluri Y *et al.* Hedgehog signaling pathway is activated in diffuse large B-cell lymphoma and contributes to tumor cell survival and proliferation. *Leukemia* 2010; **24**: 1025–36.
16 McMillan R, Matsui W. Molecular pathways: the hedgehog signaling pathway in cancer. *Clin Cancer Res* 2012; **18**: 4883–8.
17 Tompson SWJ, Ruiz-Perez VL, Blair HJ *et al.* Sequencing EVC and EVC2 identifies mutations in two-thirds of Ellis-van Creveld syndrome patients. *Hum Genet* 2007; **120**: 663–70.
18 Ruiz-Perez VL, Blair HJ, Rodriguez-Andres ME *et al.* Evc is a positive mediator of Ihh-regulated bone growth that localises at the base of chondrocyte cilia. *Development* 2007; **134**: 2903–12.
19 Dorn KV, Hughes CE, Rohatgi R. A Smoothened-Evc2 complex transduces the Hedgehog signal at primary cilia. *Dev Cell* 2012; **23**: 823–35.
20 Yamamoto K, Ishida T, Nakano K *et al.* SMYD3 interacts with HTLV-1 Tax and regulates subcellular localization of Tax. *Cancer Sci* 2011; **102**: 260–6.
21 Sasaki H, Hui C, Nakafuku M, Kondoh H. A binding site for Gli proteins is essential for HNF-3beta floor plate enhancer activity in transgenics and can respond to Shh *in vitro*. *Development* 1997; **124**: 1313–22.
22 Yamagishi M, Ishida T, Miyake A *et al.* Retroviral delivery of promoter-targeted shRNA induces long-term silencing of HIV-1 transcription. *Microbes Infect* 2009; **11**: 500–8.
23 Miyoshi H, Takahashi M, Gage FH, Verma IM. Stable and efficient gene transfer into the retina using an HIV-based lentiviral vector. *Proc Natl Acad Sci USA* 1997; **94**: 10319–23.

24 Miyoshi H, Blömer U, Takahashi M, Gage FH, Verma IM. Development of a self-inactivating lentivirus vector. *J Virol* 1998; **72**: 8150–7.
25 Kobayashi S, Nakano K, Watanabe E *et al.* CADM1 expression and stepwise downregulation of CD7 are closely associated with clonal expansion of HTLV-I-infected cells in adult T-cell leukemia/lymphoma. *Clin Cancer Res* 2014; **20**: 2851–61.
26 Sasaki D, Imaizumi Y, Hasegawa H *et al.* Overexpression of enhancer of zeste homolog 2 with trimethylation of lysine 27 on histone H3 in adult T-cell leukemia/lymphoma as a target for epigenetic therapy. *Haematologica* 2011; **96**: 712–9.
27 Smith MR, Greene WC. Identification of HTLV-I tax trans-activator mutants exhibiting novel transcriptional phenotypes. *Genes Dev* 1990; **4**: 1875–85.
28 Tsuji T, Sheehy N, Gautier VW, Hayakawa H, Sawa H, Hall WW. The nuclear import of the human T lymphotropic virus type I (HTLV-1) tax protein is carrier- and energy-independent. *J Biol Chem* 2007; **282**: 13875–83.
29 Lauth M, Bergström A, Shimokawa T, Toftgård R. Inhibition of GLI-mediated transcription and tumor cell growth by small-molecule antagonists. *Proc Natl Acad Sci USA* 2007; **104**: 8455–60.
30 Blair HJ, Tompson S, Liu YN *et al.* Evc2 is a positive modulator of Hedgehog signalling that interacts with Evc at the cilia membrane and is also found in the nucleus. *BMC Biol* 2011; **9**: 14.
31 Ego T, Ariumi Y, Shimotohno K. The interaction of HTLV-1 Tax with HDAC1 negatively regulates the viral gene expression. *Oncogene* 2002; **21**: 7241–6.
32 Kamoi K, Yamamoto K, Misawa A *et al.* SUV39H1 interacts with HTLV-1 Tax and abrogates Tax transactivation of HTLV-1 LTR. *Retrovirology* 2006; **3**: 5.

Supporting Information

Additional supporting information may be found in the online version of this article:

Fig. S1. HTLV-1 *HBZ* does not affect EVC expression.

Fig. S2. EVC knockdown reduces ATL cell proliferation.

Methods S1. Including: details of clinical samples; and primer sequences used in the present study.

Firouzi et al. Genome Medicine 2014, 6:46
http://genomemedicine.com/content/6/6/46

Genome Medicine

METHOD Open Access

Development and validation of a new high-throughput method to investigate the clonality of HTLV-1-infected cells based on provirus integration sites

Sanaz Firouzi[1], Yosvany López[2], Yutaka Suzuki[2], Kenta Nakai[3], Sumio Sugano[1], Tadanori Yamochi[1*] and Toshiki Watanabe[1*]

Abstract

Transformation and clonal proliferation of T-cells infected with human T-cell leukemia virus type-I (HTLV-1) cause adult T-cell leukemia. We took advantage of next-generation sequencing technology to develop and internally validate a new methodology for isolating integration sites and estimating the number of cells in each HTLV-1-infected clone (clone size). Initial analysis was performed with DNA samples from infected individuals. We then used appropriate controls with known integration sites and clonality status to confirm the accuracy of our system, which indeed had the least errors among the currently available techniques. Results suggest potential clinical and biological applications of the new method.

Background

It has been more than 30 years since human T-cell leukemia virus type-I (HTLV-1) was shown to be the causative agent of adult T-cell leukemia (ATL) [1,2]. However, understanding the true nature of the multiple leukemogenic events [3] that are essential for this aggressive transformation remains elusive [4-9]. Although approximately 5% of HTLV-1-infected individuals develop ATL after a long latency period, the majority remain asymptomatic carriers (ACs) throughout their lifetimes. However, there are not enough clear determinants to distinguish between individuals who eventually develop ATL and those who remain as ACs [10,11]. To discover the factors associated with disease development, long-term prospective studies have assessed the correlation between disease outcome and proviral load (PVL), that is, the percentage of infected cells among the total peripheral blood mononuclear cells (PBMCs) [10-12]. The 'Joint Study on Predisposing Factors of ATL Development' (JSPFAD) [13] showed that a PVL higher than 4% is one of the indications of risk for progression to ATL [10]. Although an elevated PVL is currently the best characterized factor associated with a high risk of ATL development, a high PVL alone is not sufficient for disease prediction, suggesting the need to discover additional predictive factors [10,11].

Because ATL is a malignancy caused by HTLV-1 infection, both the integration of provirus into the host genome and the clonal expansion of infected cells are highly critical leukemogenic events [6,7,14,15]. Although many studies have addressed these aspects, the mechanism of HTLV-1 clonal expansion has not been elucidated [15-35]. Accurate monitoring for changes in clonality occurring before, during, and after ATL development is of great interest and of major clinical significance not only to clarify the underlying mechanisms but also to discover reliable predictive biomarkers for disease progression.

A broad range of evidence strongly supports that most neoplasms are composed of clonally expanded cell populations [36-38]. Owing to its biological significance, the concept of clonal expansion in cancer biology has been investigated using a variety of approaches in many tumor types [36-39], including ATL [6,15,16,18-20,22,24,29-32].

* Correspondence: yamochi@mgs.k.u-tokyo.ac.jp; tnabe@k.u-tokyo.ac.jp
[1]Department of Medical Genome Science, Graduate School of Frontier Sciences, The University of Tokyo, 4-6-1 Shirokanedai, Minato-ku, Tokyo 108-8639, Japan
Full list of author information is available at the end of the article

Clonal proliferation of HTLV-1-infected cells was first detected as monoclonal-derived bands by southern blotting [33]. Early studies found that monoclonal integration of HTLV-1 is a hallmark of ATL cells [16]. Furthermore, it was suggested that detecting a monoclonal band is useful for diagnosis and is associated with a high risk of ATL development [29,30]. Subsequent PCR-based methods included inverse PCR, linker-mediated PCR, and inverse long PCR, which enabled analysis of samples with clonality below the detection threshold of southern blotting [17,25,31,34]. Based on the observed banding patterns, the clonality of the samples was described as having undergone monoclonal, oligoclonal, or polyclonal expansion. Such PCR-based analyses revealed that, in addition to a monoclonal proliferation of infected cells, a monoclonal or polyclonal proliferation occurs even in non-malignant HTLV-1 carriers [31,35]. Moreover, considering the stability of the HTLV-1 proviral sequence, it was hypothesized that maintaining a high PVL is achieved by persistent clonal proliferation of infected cells *in vivo* [25]. This hypothesis was further supported by the detection of a particular HTLV-1 clone in the same carrier over the course of several years [18]. Two Miyazaki cohort studies focused on the maintenance and establishment of clonal expansion: Okayama *et al.* analyzed the maintenance of a preleukemic clone in an AC state several years prior to ATL onset [19], and Tanaka *et al.* assessed the establishment of clonal expansion by comparing the clonality status of long-term carriers with that of seroconverters. They showed that some of the clones from long-term carriers were stable and large enough to be consistently detectable by inverse long PCR; however, those from seroconverters were unstable and rarely detectable over time [20].

Knowledge provided by conventional studies has shed light on the next challenges worthy of further investigation. Owing to technical hurdles, however, previous studies isolated small numbers of integration sites from highly abundant clones and detected low abundant clones in a non-reproducible manner [22,34]. Furthermore, conventional techniques could not provide adequate information regarding the number of infected cells in each clone (clone size) [22]. To effectively track and monitor HTLV-1 clonal composition and dynamics, we considered devising a new method that would not only enable the high-throughput isolation of integration sites but also provide an accurate measurement of clone size.

PCR is a necessary step for the integration site isolation and clonality analysis. However, bias in the amplification of DNA fragments (owing to issues such as extreme fragment length and high GC content) is intrinsic to any PCR-based method [40-45]. Different fragment amplification efficiencies make it difficult to calculate the amount of starting DNA (the original distribution of template DNA) from PCR products. Hence, estimating HTLV-1 clonal abundance, which requires calculating the number of starting DNA fragments, is only achievable by avoiding the PCR bias.

Recently, Bangham's research group analyzed HTLV-1 clonality and integration site preference by a high-throughput method [22]. In the method developed by Gillet *et al.*, clone sizes were estimated using length of DNA fragments (shear sites generated by sonication) as a strategy for removing PCR bias [22]. Owing to the limited variation in DNA fragment size observed with shearing, the probability of generating starting fragments of the same lengths is high, leading to a nonlinear relationship between fragment length and clone size [22,46]. Therefore, Gillet *et al.* used a calibration curve to statistically correct the shear site data [22]. Later, Berry *et al.* introduced a statistical approach, and further addressed the difficulties of estimating clone size from shear site data [46]. Their approach estimates the size of small clones with little error, but estimates for larger clones have greater error [46]. A parameter adopted from the Gini coefficient [47,48] and termed the oligoclonality index was used to describe the size and distribution of HTLV-1 clones [22]. It has been demonstrated that the oligoclonality index differs between malignant and non-malignant HTLV-1 infections, and also a high PVL of HTLV-1-associated myelopathy is due to cells harboring large numbers of unique integration sites [22]. Furthermore, genome-wide integration site profiling of clinical samples revealed that the abundance of a given clone *in vivo* correlates with the features of the flanking host genome [22,24]; although there was not a specific hotspot, HTLV-1 more frequently integrated in transcriptionally active regions of the host genome [22,24]. These findings further clarified the characteristics of HTLV-1 integration sites, and strongly suggested the importance of HTLV-1 clonal expansion *in vivo*.

Here we introduce a method that overcomes many of the limitations of currently available methods. Taking advantage of next-generation sequencing (NGS) technology, nested-splinkerette PCR, and a tag system, we designed a new high-throughput method that enables specific isolation of HTLV-1 integration sites and, most importantly, allows for the quantification of clonality not only from the major clones and high-PVL samples but also from low-abundance clones (minor clones) and samples with low PVLs. Moreover, we conducted comprehensive internal validation experiments to assess the effectiveness and accuracy of our new methodology. A preliminary validation was conducted by analyzing DNA samples from HTLV-1-infected individuals with different PVLs and disease status. Subsequently, an internal validation was performed that included an appropriate control with known integration sites and clonality patterns. We present our methodology, which illustrates

that employing the tag system is effective for improving quantification of clonal abundance.

Methods

Our clonality analysis method included two main aspects: (1) wet experiments, and (2) *in silico* analysis (Additional file 1: Figure S1). A general explanation of materials and methods is provided here, and detailed protocols of the wet experiments are included in Additional file 1: Notes. The *in silico* analysis is further described in Results and discussion.

NGS data have been deposited in the Sequence Read Archive of NCBI with access number of (SRP038906).

Wet experiments

Biological samples: specimens and cell lines

Specimens: In total five clinical samples were provided by a biomaterial bank of HTLV-1 carriers, JSPFAD [13,49]. The clinical samples were a part of those collected with an informed consent as a collaborative project of JSPFAD. The project was approved by the Institute of Medical Sciences, the University of Tokyo (IMSUT) Human Genome Research Ethics Committee. Information about the disease status of samples was obtained from JSPFAD database in which HTLV-1-infected individuals were diagnosed based on the Shimoyama criteria [50]. In brief, genomic DNA from PBMCs was isolated using a QIAGEN Blood kit. PVLs were measured by real-time PCR using the ABI PRISM 7000 Sequence Detection System as described in [10].

Cell lines: An IL2-dependent TL-Om1 cell line [51] was maintained in RPMI 1640 medium supplemented with 10% heat-inactivated fetal calf serum (GIBCO), 1% penicillin-streptomycin (GIBCO), and 10 ng/mL IL2 (R&D systems). The same conditions as those of patient samples were used to extract DNA and measure PVL.

Illumina-specific library construction

We employed a library preparation protocol specifically designed to isolate HTLV-1 integration sites. The final products in the library that we generated contained all the specific sequences necessary for the Illumina HiSeq 2000 platform (Additional file 1: Figure S2). These products included a 5′-flow cell binding sequence, a region compatible with read-1 sequencing primer, 5-bp random nucleotides, 5-bp known barcodes for multiplexing samples, HTLV-1 long terminal repeat (LTR), human or HTLV-1 genomic DNA, a region compatible with read-2 and read-3 sequencing primers, 8-bp random tags, and a 3′-flow cell binding sequence from 5′ to 3′, respectively (Additional file 1: Figure S2B).

Incorporating the 5-bp random nucleotides downstream of the region compatible with the read-1 sequencing primer was critical and resulted in high-quality sequence data. We used a library designed without the first 5-bp of random nucleotides as input for the HiSeq 2000 sequencer in our first samples (S-1, S-2, S-3, and S-4). Because all fragments began with the same LTR sequence, clusters generated in the flow cells could not be differentiated appropriately. These samples resulted in low-quality sequence data (see Additional file 1: Notes). Designing the first 5-bp randomly resulted in high-quality sequence data for the remaining samples because clusters were differentiated with no problem during the first five cycles of sequencing (data not shown).

Our library construction pipeline comprised the following four steps (Additional file 1: Figure S2) (Additional file 1: Notes):

(1) DNA isolation: DNA was extracted as described above, and the concentration of extracted DNA was measured with a NanoDrop 2000 spectrophotometer (Thermo Scientific). We recommend using 10 μg of DNA as the starting material. However, in practice there are some rare clinical samples with limited DNA available. In order to be able to handle those samples, the method was also optimized for 5 μg and 2 μg of starting DNA.
(2) Fragmentation: According to the protocol provided in Supplementary Notes, the starting template DNA was sheared by sonication. The resulting fragments represented a size range of 300 to 700 bp as checked by an Agilent 2100 Bioanalyzer and DNA 7500 kit (Figure 1B).
(3) Pre-PCR manipulations: Four steps of end repair, A-tailing, adaptor ligation, and size selection were performed as described in Additional file 1: Notes.
(4) PCR: To amplify the junction between the genome and the viral insert, we used nested-splinkerette PCR (a variant of ligation-mediated PCR [52,53]) (Additional file 1: Figure S2). We confirmed that the technique specifically amplifies HTLV-1 integration sites; since there was no non-specific amplification neither from human endogenous retroviruses nor from an exogenous retrovirus such as HIV (see Additional file 1: Table S1 and Additional file 2: Figure S1).

Information on oligonucleotides, including adaptors and primers, and the LTR and HTLV-1 reference sequences [54] are provided in Additional file 1: Table S1. The final PCR products were sequenced using the HiSeq 2000 platform.

In silico analysis

Raw sequencing data were processed according to the workflow described in the Results and discussion section.

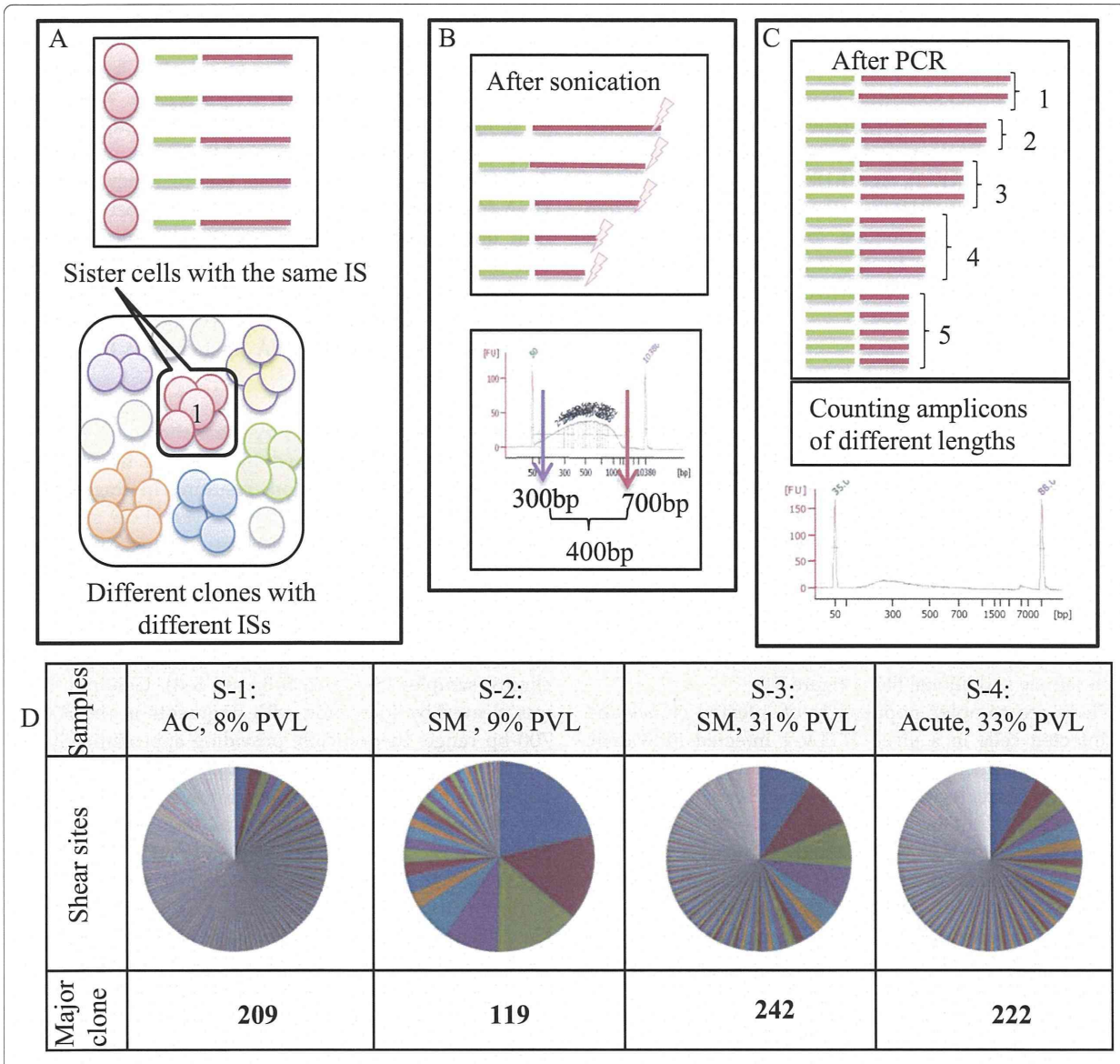

Figure 1 Estimating clone size by 'shear sites'. Also see Additional file 2: Figure S2 for a simple image from an integration site and its shear sites. **(A)** Depicted is the complex population of uninfected cells (grey circles) together with infected clones (circles of different colors). A clone is shown as a group of sister cells (circles of the same color) having the same integration site (IS). Different clones are distinguishable based on differing integration sites, and thus the number of integration sites represents the number of infected clones. For example, the six different unique integration sites refer to six unique clones. **(B)** Genomic DNA fragmented by sonication generates random shear sites (fragments of different length). Fragment size, measured by an Agilent Bioanalyzer, ranged from 300 to 700 bp. This size range can theoretically provide approximately 400 variations. **(C)** The size distribution of fragments decreased following amplification by integration-site-specific PCR. From the deep sequencing data, the original number of starting fragments could be estimated by removing PCR duplicates and counting fragments with different lengths. For example, five different lengths of PCR amplicons represent five infected sister cells. **(D)** We analyzed four samples, including (S-1: asymptomatic carrier (AC), (8% PVL)), (S-2: smoldering (SM), (9% PVL)), (S-3: smoldering, (31% PVL)), and (S-4: acute, (33% PVL)). Using our method, the clone sizes were quantified by considering only shear sites. The first major clone (the largest clone) of each sample was mapped to (chr 11-41829319 (+)), (chr 15: 59364370 (+)), (chr 4-563543 (-)), and (chr X - 83705328 (-)), respectively. The shear site variations of each major clone were 209, 119, 242, and 222, respectively. Different colors on the pie graphs indicate different integration sites, and the size of each piece represents the clone size.

The initial forward read (100-bp) was termed Read-1 and the reverse read (100-bp) was termed Read-3 and an index read (8-bp) was termed Read-2. In brief, analysis programs were written in Perl language and run on a supercomputer system provided by The University of Tokyo's Human Genome Center at The Institute of Medical Science [55]. The sequencing output was check for quality using the FastQC tool [56]. The regions corresponding to the LTR

and HTLV-1 genome were subjected to a blast search against the reference sequences described in Additional file 1: Table S1. Following isolation of the integration sites, the flanking human sequences were mapped to the human genome (hg19) (the UCSC genome browser [57]) by Bowtie 1.0.0 [58]. The final processed data included information about shear sites (R1R3), tags (R1R2), and a combination of tags and shear sites (R1R2R3). Fitting the data to the zero truncated Poisson distribution for retrieving correlation coefficients were done by the R-package 'gamlss.tr' [59]. The Gini coefficient was calculated by StatsDirect medical statistics software [60].

Results and discussion

General concepts

We originally designed our method to overcome the limitations of conventional techniques [31,34] and to make improvements in the only existing high-throughput method [22]. In general, our method includes two main sets of wet experiments and an *in-silico* analysis. We used genomic DNA as the starting material to prepare an appropriate library for Illumina sequencing. Subsequently, deep-sequencing data were analyzed by a supercomputer. The resulting information represents the clonality status of each sample (Additional file 1: Figure S1).

There are complex populations of infected clones and uninfected cells in a given HTLV-1 infected individual. High-throughput clonality analysis requires monitoring two main characteristics of clones: HTLV-1 integration sites and the number of infected cells in each clone (clone size). Each HTLV-1-infected cell naturally harbors only a single integration site [23]. Therefore, the number of detected unique integration sites corresponds to the number of infected clones. Based on our analysis, which is consistent with the data of Gillet *et al.* [22], employing high-sensitivity deep sequencing allowed for the isolation of a large number of unique integration sites (UISs), including samples with low PVLs (Figure 1). We analyzed four samples from HTLV-1-infected individuals with different PVLs, disease status, and expected clonality patterns. The samples include S-1: AC (8% PVL); S-2: smoldering ATL (SM) (9% PVL); S-3: SM (31% PVL); and S-4: acute ATL (33% PVL). Based on the final optimized conditions, 1030, 39, 265, and 384 UISs were isolated from each sample, respectively (Figure 1).

The most challenging aspect of our clonality analysis was estimating the number of infected cells in each clone. Although a necessary step in the analysis, PCR introduces a bias in the frequency of starting DNA material [40-45]. Because amplification causes significant changes in the initial frequency of starting materials, PCR products cannot be used directly to estimate the amount of the starting DNA material. To overcome this problem, we needed to manipulate DNA fragments to make them unique prior to PCR amplification. Thus, if each DNA fragment could be marked with a unique feature, it would then be possible to calculate its frequency based on the frequency of that unique feature. When a single unique stretch of DNA is amplified by PCR, the resulting product is a cluster of identical fragments termed PCR duplicates. Therefore, to estimate the frequency of starting DNA fragments, one should count the number of clusters with unique features. The remaining technical question then becomes how to mark the starting DNA prior to PCR amplification. In the following section, we compare and discuss two main strategies, namely (1) shear sites and (2) a tag system, which enable DNA fragments to be uniquely marked.

Estimating the size of clones by shear sites

The first strategy, described by Gillet *et al.*, relies on shearing DNA by sonication, resulting in fragments of random length [22]. Sonication-derived shear sites were thus used as a distinguishing feature to make fragments unique prior to PCR. Clone sizes were then estimated by statistical approaches [22,46].

To directly assess the effectiveness of the shear site strategy, we analyzed the clonality of the aforementioned clinical samples (S-1, S-2, S-3, and S-4). Genomic DNA was cleaved by sonication with fragments in the 300- to 700-bp range, theoretically providing approximately 400 possible variations in fragment size (Figure 1A and B). Following library construction, however, the final product represented smaller size ranges, implying a relatively limited number of variations (Figure 1C). Finally, the number of PCR amplicons with unique shear sites was retrieved from deep-sequencing data. See Additional file 2: Figure S2 for a simple image from an integration site and its shear sites. The data obtained from the shear site experiments were not fitted to calibration curves or statistical treatments, which were used by Gillet *et al.* and Berry *et al.*, respectively (See Additional file 1: Notes) [22,46]. For clarity, only the information relating to the major clone of each sample is provided in Figure 1D. The shear-site variations of the major clone were 209, 119, 242, and 222 for samples S-1 through S-4, respectively. Even in the case of control samples with 100% PVLs, the shear sites did not provide more than 225 variations (see Validation of the methodology). However, it was expected that samples with differing PVLs and disease status would harbor varying numbers of sister cells, at least in their major clones. Similar variations of shear sites were observed in major clones of AC, SM, and acute samples. These data suggest that, because the number of sister cells in each clone exceeded the shear site variations, the size of the clones was underestimated (Figure 1). This is most problematic in the case of large clones and leads to an underestimation of the clone size.

Measuring the size of clones by the tag system

We developed an alternate strategy to remove PCR bias and to estimate starting DNA. We designed a tag system in which 8-bp random nucleotides are incorporated at the end of DNA fragments during adaptor ligation step. Each tag acts as a molecular barcode, which gives each DNA fragment a unique signature prior to PCR. Information on the frequency of observed tags from the deep-sequencing data can be used to remove the PCR duplicates and thereby estimate the original clonal abundance in the starting sample. Owing to their random design, the tags could theoretically provide approximately 65,536 variations. This degree of potential variation is expected to provide a unique tag for a large number of sister cells in each clone (Figure 2).

We analyzed samples S-1, S-2, S-3, and S-4 to assess the effectiveness of our tag system for estimating clone size. The major clone of each sample showed tag variations of 393, 142, 1751, and 2675, respectively (Figure 2D). Similar variations of tags and shear sites were observed in the

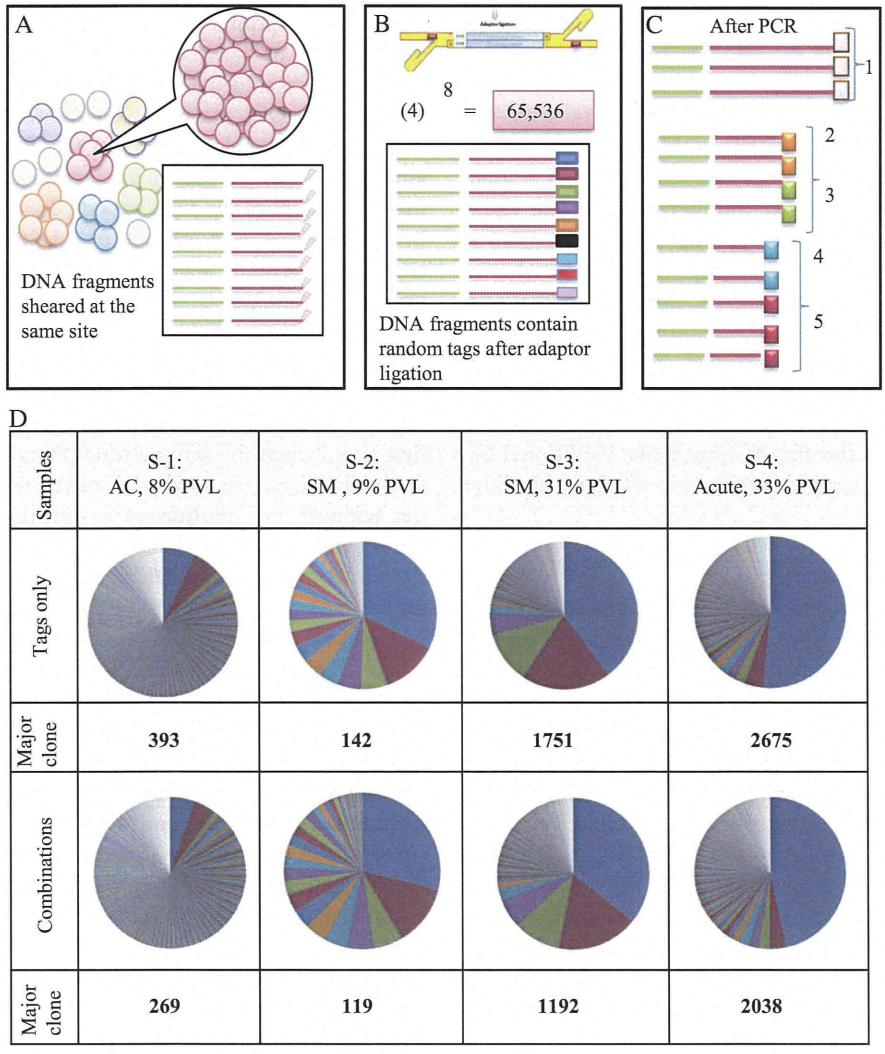

Figure 2 Measuring clone size using the tag system. (A) The depiction above shows that shear site variations are not able to cover all sister cells in large clones. As the number of the sister cells in a given clone increases, the probability of DNA shearing at the same site increases. **(B)** Prior to PCR, we incorporated 8-bp random tags into each DNA fragment to uniquely mark them. Random tags could theoretically provide approximately 65,536 variations. The number of potential variations is expected to amply cover large numbers of the sister cells. **(C)** The tag information was used to remove PCR duplicates and to estimate the original number of starting fragments. If the fragments had the same shear sites but different tags, they were counted separately. For example, here five different combinations of tags and shear sites represent five infected cells. **(D)** Samples: S-1, S-2, S-3, and S-4 were analyzed by the final optimal condition (Bowtie parameters: -v 3 - - best, and filtering condition: (merging approach) JT-10). Clone size was measured by tags only or by the combination of shear sites and tags. The covered variations were (393,142, 1751, and 2675) and (269, 119, 1192, and 2038), respectively.